Materials and Structures (2017) 50:194
DOI 10.1617/s11527-017-1062-2

ORIGINAL ARTICLE

Effects of waste glass on alkali-activated tungsten mining waste: composition and mechanical properties

Gediminas Kastiukas · Xiangming Zhou

Received: 13 February 2017 / Accepted: 7 June 2017 / Published online: 22 June 2017

Abstract Increasingly more research is being directed towards the valorisation of waste materials as precursors for synthesising alkali-activated binders (AABs). For this study, varying blends of tungsten mining waste (TMW) and waste glass (WG) are activated using a combined sodium hydroxide (SH) and sodium silicate (SS) alkali solution. The activating solution itself is also varied with respect to the quantities of SS and SH to determine their effect on reactant formation and mechanical strength of TMW-based AABs. The results show that an increased WG content can effectively provide an additional source of reactive silica, contribute to the formation of (C, N)–A–S–H gel products and thus significantly improve the mechanical strength. High strength TMW–WG AABs were attributed to a faster TMW dissolution rate and dense microstructure. Such structures were characteristic of formulations with low alkali modulus (SiO_2/$Na_2O < 2$) combined with a SS/SH weight ratio of 2.8. For the latter, not only was a characteristic slower strength development with increasing alkali content observed, but there was also a limit of alkali metal concentration ($Na_2O \sim 3.1\%$) beyond which the strength deteriorated. Furthermore, SEM micrographs disclose that unreacted particles of WG reinforced the matrix by acting as a filler.

Keywords Alkali-activation · Geopolymer · Microstructure · Recycling · Tungsten mining waste · Waste glass

G. Kastiukas · X. Zhou (✉)
Department of Mechanical, Aerospace and Civil Engineering, Brunel University London, Uxbridge UB8 3PH, UK
e-mail: Xiangming.Zhou@brunel.ac.uk

G. Kastiukas
e-mail: Gediminas.Kastiukas@brunel.ac.uk

1 Introduction

Research into the production of alternative cementitious materials via a chemical activation process over the last 40 years has proven to be very promising with the outcomes being industrial patents [1, 2] and construction projects [3, 4]. Chemically activated binders are typically Portland cement-free and their production can be considered to consist of a five-stage process: (1) dissolution of solid aluminosilicate source by alkali species in activating solution, (2) rearrangement and exchange among dissolved species, (3) gel nucleation [C–(A)–S–H or N–A–S–(H) gel], (4) solidification and hardening, and (5) ongoing gel evolution [5]. The resulting benefits include high strength with rapid setting, good durability and high resistance to chemical attack [6–8]. An obvious advantage of chemically activated binders, compared to the conventional Portland cement binders, is the ability to conveniently dispose of the variety of waste material available from multiple industries. Typical

aluminosilicate material sources suitable for chemical activation can include industrial waste by-products such as fly ash and slag [9] and calcined clays such as metakaolin [10]. Currently, increased interest has been directed towards developing new binders based on non-conventional precursor materials [11]. In particular, tungsten mining waste (TMW) is one type of aluminosilicate precursor which has had little research coverage regarding chemical activation. The stimulus for its re-use lies in the environmental impact of mining and quarrying activities, which in the EU generate approximately 735 million tonnes of waste per annum, contributing to 30% of the total waste generation by economic activity and households [12]. Preliminary studies have been conducted on the transformation of tungsten mining waste into alkali-activated binders (AABs) and have shown promising results from an environmental, technical and economic point of view [13, 14]. In addition to mining waste, post-consumer waste glass (WG) represents another major component of the solid waste stream. Today, waste glass has also become a substantial burden on the landfills throughout the world, and it is estimated that out of 18 million tonnes of glass wastes accumulated in 2012 in the EU, only 35% of this was recycled [15]. The feasibility of waste glass to improve mechanical performance has been achieved with PC concrete [16] and metakaolin based AABs [17]. Soluble nanosilica has also been used as an alternative activator in alkali-activated fly ash binders, proving to lower water demand, reduce permeability and match the compressive strength of the samples made with commercial silicate [18]. Thus, in summary, the disposal and recycling of both mining waste and waste glass have become a major concern in the EU due to the lack of the sustainable initiative. As a result, it is essential to find a suitable method for their reuse in the production of chemically activated binders.

In chemically-activated cementitious systems, large additions of strong alkaline activators are needed, which may pose health risks, especially when such binders are used in dry mix mortar formulations (e.g. tile adhesives), where the workers get into contact with the highly alkaline material. The cost of manufacture and associated health risks make highly alkaline conditions unreasonable and one of the principle drawbacks of alkali-activated binder systems. The use of less concentrated activators including alkali carbonates and sulphates [19–22] and organic activators with carboxylate groups as summarised in [23] has been reported previously. Alternatively, activation using phosphoric acid has also shown promising results regarding durability with excellent resistance to elevated temperatures [24]. The presence of soluble silica is also known to improve the mechanical properties of the resulting AABs [25] at early ages. Fernández-Jiménez et al. [26] found that different types of fly ash activated with 8–12 M NaOH yielded a material with mechanical strength ranging from 35 to 40 MPa, and up to 90 MPa when waterglass was added to the NaOH solution [27]. Nevertheless, there is a lack of detailed studies of using waste silicate materials to supplement the chemical activation. Previous research has established that SiO_2 is highly soluble in alkaline solutions making the SiO_2/Na_2O molar ratio an important parameter of AABs [28] while the composition and dosage of the activating solution also plays a critical role in controlling the gelation process [29]. In this contribution, a study of the interaction of the tungsten mining waste replaced by varying proportions of siliceous waste glass is discussed. The first stage of the study is a report on the effects of increased replacement of TMW by WG. In the second stage of the paper, a systematic study of the effects of the individual sodium hydroxide and sodium silicate components of a multi-compound alkali activator is reported. Scanning electron microscopy is used to characterise the hardening process and structural composition of the final products while compressive strength tests at specific ages are made to determine the mechanical strength.

2 Materials and methods

2.1 Materials

TMW obtained from the Panasqueira mine, Portugal and a siliceous WG obtained from the Covilhã local authority were used as the precursor materials. Due to the waste nature of the TMW, chemical analyses were made from different batches collected from the mine over the course of this study. Hence the mean chemical composition of TMW (including its standard deviation (SD)) and WG in wt% are presented in Table 1. Both materials were dried, milled and sieved to achieve a mean particle size of 26 and 39 μm respectively. The

Table 1 Chemical composition of TMW and WG

Chemical compound	TMW (%)	TMW SD (%)	WG (%)
Na_2O	1.31	1.45	9.72
MgO	1.01	2.98	0.00
Al_2O_3	21.06	2.53	0.00
SiO_2	47.88	3.86	73.93
SO_3	8.72	2.83	0.00
K_2O	4.12	0.78	0.69
Fe_2O_3	9.97	2.73	0.40
P_2O_5	0.00	0.27	0.00
CaO	0.88	0.99	12.83
TiO_2	0.66	0.35	0.00
LOI	4.19		0.08

WG was intentionally used with a larger mean particle size to reduce the energy expended during the milling process; however, due to the high alkali-silica reactivity of crushed glass [30], particle size was maintained below 100 μm to prevent the onset of this reaction. A commercial sodium silicate (Na_2SiO_3) (SS) solution with composition $SiO_2/Na_2O = 3.23$ (8.60 wt% Na_2O, 27.79 wt% SiO_2, 63.19 wt% H_2O and 0.4 wt% Al_2O_3) (Solvay S.A) and 99% pure sodium hydroxide (NaOH) (SH) pellets (Sigma-Aldrich) were used for the production of the alkali activator.

2.2 Experimental process

For Stage I of the study, TMW AAB samples were synthesised with different WG replacement levels, namely 0, 20, 30 and 40 wt% and named 100TMW, 80TMW20WG, 70TMW30WG and 60TMW40WG, respectively. The mix ratio was determined based on the research on alkali-activation available in the literature concerning mechanical strength and efflorescence formation potential in AABs combined with the experience gained from a previous study [31]. In summary, the following ratios were selected for the constituents of the AABs in Stage I:

- Silicate modulus = 1.75 (molar ratio)
- $\%Na_2O = 3.63$ (mass ratio)
- Water/precursor = 0.18 (mass ratio)

During Stage II, the TMW AAB with a WG replacement level that provided the highest compressive strength at 28 days from Stage I of the study was used to investigate the alkali activator composition, as shown in Table 2. Samples in Table 2 are expressed in terms of the activator/precursor ratio (*a*/*p*), $\%Na_2O$ content and silicate modulus (Ms) i.e. SiO_2/Na_2O. Researchers have investigated the identification of optimum Ms values for precursor materials such as fly ash [32] and metakaolin [33], for which the chemical composition of the alkaline solution favours the compressive strength. This suggests that in addition to factors such as the nature of the precursor materials and the curing conditions, the Ms is also a significant parameter in strength development and workability. Ms has been used to give insight into the pH of the activator solution, its viscosity, the structural complexity of the Si soluble species present in the alkaline solution [34], and in turn, can be related to the process of dissolution and condensation of reaction products.

Table 2 Mix proportions of the alkali-activated TMW/WG blends

Sample	*a*/*p* (g/g)	Na_2O (%)	Ms (g/mol)
1	0.24	2.5	2.51
2	0.26	3.1	2.00
3	0.28	3.7	1.69
4	0.3	4.4	1.45
5	0.32	5	1.27
6	0.34	5.6	1.13
7	0.22	3.1	1.48
8	0.25	3.4	1.62
9	0.28	3.6	1.75
10	0.31	3.8	1.85
11	0.34	4.1	1.94

A 10 M SH solution was prepared by dissolution of NaOH pellets in purified water and stored for a minimum of 24 h before use, to allow equilibration; SS solution was used as received from the manufacturer. Both solutions were kept in sealed containers whenever possible to minimise contamination by atmospheric carbonation. SH and SS solutions were combined and mixed using a magnetic stirrer for 5 min at 400 rpm.

The AAB samples were prepared by mechanically mixing mass ratio quantities of TMW and WG with alkali activator solution in a benchtop laboratory mixer in the following sequence: 2.5 min at 100 rpm; 30-s pause to remove material adhered to the sides of the mixing bowl; 2 min at 200 rpm. The paste was

vibrated for a further 5 min to remove entrained air before being transferred to prismatic 40 × 40 × 160 mm^3 Styrofoam moulds. Samples were kept sealed from the atmosphere in vacuum bags and cured in accordance to the previously determined optimal temperature and duration of 80 °C and 24 h [35], respectively. After that, the samples were demoulded and stored at 20 °C and relative humidity of 90% until use for mechanical strength tests.

2.3 Testing methods and conditions

The compressive strength of the samples was determined in accordance with EN 196-1 using a universal testing machine (Instron 5960) at a constant loading rate of 144 kN/min. Prismatic sample fractured counterparts were tested after 1, 3, 7, 28 days. The reported compressive strength result was the average of values obtained from three specimens with the error reported as average deviation from the mean; the deviation of results fluctuated between 0.22 and 1.4%.

The setting time of the TMW–WG AAB was measured according to EN 196-3 [36]. The samples were kept in the curing chamber at 80 °C in between measurements and setting were measured from the time the precursor materials made contact with the activating solution until the penetration of a 2 mm diameter needle reached a depth of 10 mm. The reported setting time results were the average of three samples. The flow test cone with an internal diameter of 100 mm was used to evaluate the fluidity of TMW–WG AAB as described by EN 1015-3:1999 [37]. Before the test, the truncated cone mould was placed on a clean metal plate, and the freshly prepared TMW–WG AAB mixture was poured into the cone without any compaction. Once the cone was fully filled with the sample, the cone was lifted vertically, and the spread diameters of the freshly prepared sample in two perpendicular directions were measured. All flow test measurements were conducted 7 min after mixing and the occurrence of bleeding, if any, was visually observed and noted during the test.

Electron microscopy was performed using a Zeiss Supra 35VP using backscattered electron (BSE) mode combined with energy-dispersive X-ray (EDX) spectroscopy to analyse the sample morphology and microstructure. Samples were impregnated in low viscosity epoxy resin and polished using consecutively finer media. The polished sample surfaces were coated using a gold sputter coater to eliminate effects of charging during micrograph collection. SEM samples were tested in a state where the alkali activation process has been stopped using the combined water and solvent extraction protocol developed by Chen et al. [38]. In summary, it involved stirring the AAB specimen in deionized water and then removing the liquid by centrifuging. Upon addition of methanol, soluble silicate species could be observed in the liquid layer. Thus water extraction by centrifuging was used to remove the precipitates. Specimens were then ground to micron-sized particles using a mortar and pestle, and a solvent of methanol/acetone mixture was added, followed by further grinding. The solvent was removed using vacuum filtration; this latter procedure was repeated for five times. The bleeding test procedure was conducted according to the reference standard EN 480-4:2005 [39]. It involved filling a cylindrical vessel with an inside diameter and height of 250 and 280 mm, respectively with fresh TMW–WG AAB binder and subsequently drawing activator solution from the surface of the test specimen every 30 min. The activator bleeding is expressed as a percentage of the total activator content.

3 Results and discussion

3.1 Stage I: influence of waste glass on mechanical performance

The early age reaction product formation in the 100TMW sample is shown in Fig. 1a. The results from the SEM imaging show sites of N–A–S–H gel reaction products (P1) with different cation and anion substitution of Fe, Mg and K which are amorphous in structure and show branch-like formations bridging the reaction products together. The same reaction products can also be seen merging with the quartz particles from the TMW, forming the gel network. In Fig. 1b, the muscovite crystals (labelled as M) in the TMW AAB is shown to develop a densely laminated structure during alkali activation indicating an uptake of hydroxyl ions due to rehydroxylation. Using EDX microanalyses, the Al/Si ratio for unreacted muscovite was determined as 1.0, while measurements made after one day of reacting with the alkali activator saw the latter value drop to 0.65, demonstrating a clear

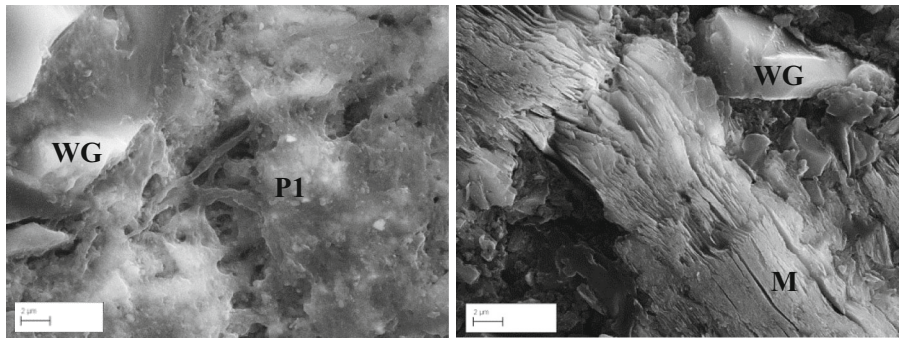

Fig. 1 TMW AAB showing **a** branch-like product formations and **b** laminated structure of muscovite

indication of the release of aluminium cations into solution.

The average compressive strength of the four different compositions of AAB with the replacement of TMW with WG by up to 40 wt% is summarised in Fig. 2. The results obtained for pure TMW AAB are also included. In Fig. 2 it can be observed that the compressive strength increased with an increase in the WG content across all ages. The replacement by 40 wt% WG i.e. sample 60TMW40WG, resulted in a 16% increase in SiO_2 molar content and resulted in the highest 28-day compressive strength of 41 MPa; a 127% increase relative to the 100TMW control sample. The early age compressive strength attainment was also observed to improve with the increase in WG. Starting with the control sample of 100TMW, the compressive strength at 1-day is only 12.3% of the final 28-day strength. However, for 20, 30 and 40 wt% replacement of TMW by WG, the 1-day strength increases to 48.6, 67.8 and 72% of the final 28-day strength. To explore the latter strength increments, SEM micrographs of AAB revealing the microstructural differences in samples made with WG are shown in Fig. 3. TMW particles in the 1-day 60TMW40WG sample (Fig. 3a) exhibited more regions of the muscovite crystal with a laminated structure (identified by the lighter regions) which can be inferred as in increase in the level of Al and Si leaching. On the other hand, the muscovite particle in the 1-day 100TMW sample (Fig. 3b) remained relatively unchanged. The 60TMW40WG sample structure appears to contain fewer voids while the reaction products appear more dense and have more continuity i.e. are not comprised of isolated regions like in the 100TMW sample. Dense amorphous gel formations were also observed in the 60TMW40WG (Fig. 3c). The latter figure also shows how particles of WG are partially transforming into amorphous reaction products supporting the idea that an increased replacement of WG provides a means of increasing reactive silica and thus increasing the Si/Al ratio; this means less reliance on using the more costly and less sustainable soluble silica found in commercial sodium silicate solution. By the age of 28 days, many large particles of SiO_2 were found embedded in the AAB matrix (shown in Fig. 3d). However it was difficult to establish the quantity that came from the TMW and WG. Nonetheless, it can be inferred that the increased WG content may not have only supplied reactive silica to the mix but also contributed to strengthening the AAB as inert filler, most likely by the coarser fraction of WG.

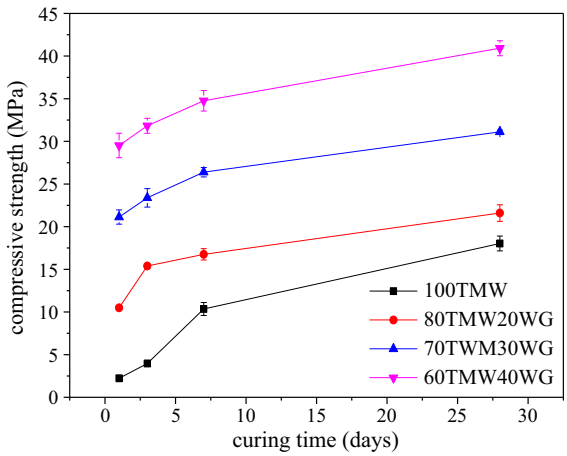

Fig. 2 Effects of WG substitution on compressive strength

Further interpretation can be made from Fig. 4, which shows the Energy Dispersive X-ray (EDX) spectra for the 1-day reaction products in the 100TMW sample (P1) and the 60TMW40WG sample

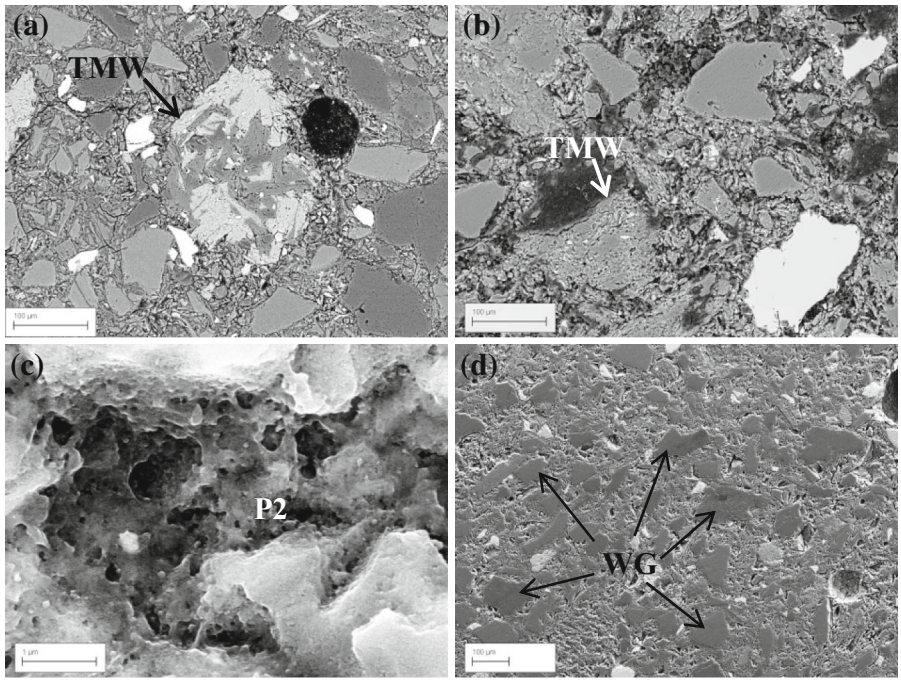

Fig. 3 SEM images of **a** 60TMW40WG, **b** 100TMW, **c** amorphous reaction products in 60TMW40WG and **d** unreacted WG particles

(P2). The distinction between the spectra is firstly the increased intensity of the main Si peak at 1.7 keV (4.5 K for P1 and 14.4 K for P2) which is due to the contribution of amorphous silica from the WG. The Si/Al molar ratio of the reaction product P1 in the 100TMW sample was measured to be 1.08, while the Si/Al molar ratio of the reaction products P2 for the sample containing a 40 wt% replacement by WG increased to 3.0. Secondly, the combination of elements for P2 in Fig. 4 can be identified as (C, N)–A–S–H gel formation. The occurrence of this gel is consistent with the observations developed through a comparable system of alkali-activated fly-ash with partial replacement with slag (rich in Si and Ca) [40]. The Ca released by WG dissolution is incorporated into the N–A–S–H type gel resulting from TMW activation and is believed to contribute to the increased mechanical strength of the 60TMW40WG sample, which is a factor previously shown to improve the mechanical properties of alkali-activated fly ash [41].

The compressive strength results with the highest replacement by WG i.e. 40 wt% are comparable with the results of Pacheco-Torgal et al. [42] who obtained 39.6 MPa at 28 days for an alkali-activated TMW mortar. However, this was achieved only after an

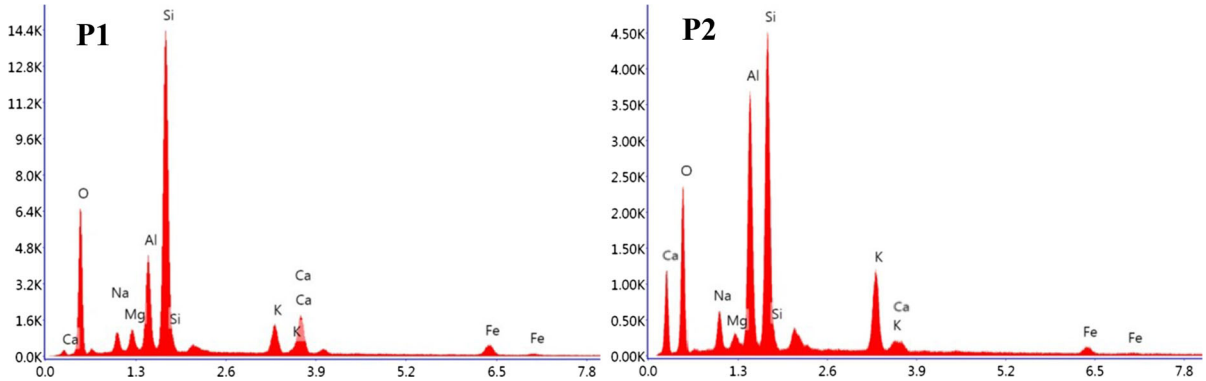

Fig. 4 SEM-EDX of **P1** in 100TMW and **P2** in 60TMW40WG

energy intensive calcination treatment of the TMW at 950 °C for 2 h.

3.2 Stage II: influence of alkali-activator composition

The results from Stage I revealed that the TMW-AAB with the highest replacement by WG i.e. 40 wt% led to the highest compressive strength. Thus it was this particular AAB composition which was chosen for further investigation in stage II of this study. Figure 5 presents the results of the 60TMW40WG AAB compressive strength with varying values of Ms i.e. SiO_2/Na_2O. Figure 5a shows the effect of an increased Ms due to SH while maintaining a constant quantity of SS, while in Fig. 5b, it is vice versa. The results reveal that the values of Ms show more variation and thus impact on the AAB strength development due to changes in the SH component of the alkali activator rather than SS. For the TMW–WG AAB samples 1–6, presented in Fig. 5a, made with a constant SS/precursor ratio of 0.22 and varying SH/precursor ratio from 0.02 to 0.12, the increase in Ms over the 1.13–2.0 range results in an increase in compressive strength across all ages. However, a further increase in Ms over the 2.0–2.51 range resulted in an immediate reduction in the 28-day compressive strength. The latter result can be related to the reduction in $\%Na_2O$ content (mass ratio of total Na_2O in the activator solution to precursor). The increase in compressive strength from 29 to 46 MPa is for a reduction of $\%Na_2O$ from 5.6 to 3.1% while the reduction in compressive strength from 46 to 42 MPa occurs when the $\%Na_2O$ falls from 3.1 to 2.5%. The charge distribution of Na alkali metal ions surrounding the Al and Si ions defines the ionic atmosphere and depends on the concentration of the Na ions. The ionic atmosphere can be thought of as a measure of the ion–ion interaction [43], in the sense that when it is much larger that the Si or Al ionic radius, the ions can be considered as point charges with reduced interaction, while if it is in the same range with the ionic radius then this can allow for stronger ion–ion interactions. Thus, the initial reduction in the alkalinity from 5.6 to 3.1% would in turn reduce the Na ionic atmosphere and improve the Al and Si interaction, allowing less interference in the creation of bonds within the aluminosilicate gel framework and increasing the degree of connectivity. The latter would also reduce the setting time, an aspect of the TMW–WG AAB discussed further on in this study.

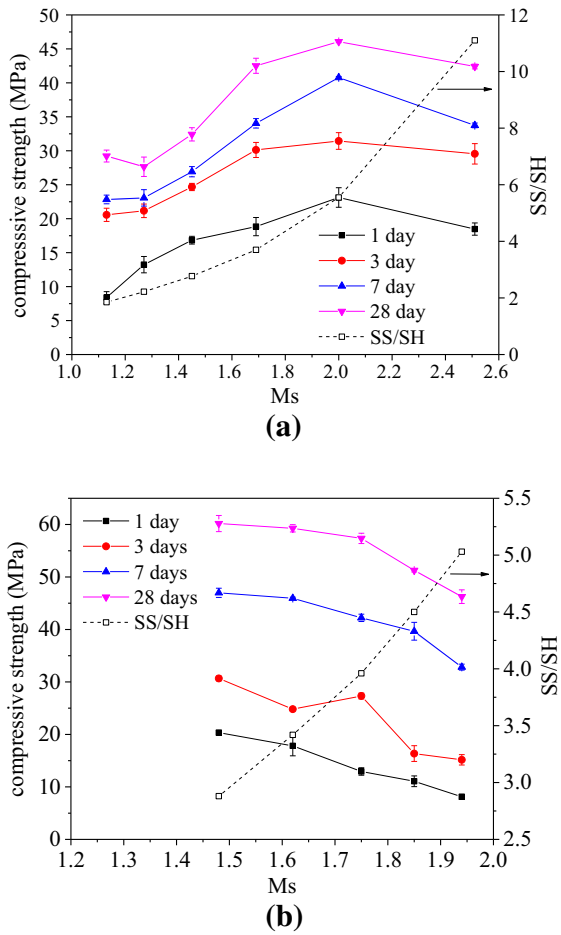

Fig. 5 Effect of varying **a** SH and **b** SS in the alkali activator

On the other hand, samples 7–11 which are presented in Fig. 5b were made with a constant SH/precursor ratio of 0.06 and an SS/precursor ratio ranging from 0.16 to 0.28. The increase in $\%Na_2O$ for these samples was over a smaller range (3.1–4.1%) and thus impacted the compressive strength to a lower degree. Sample 7, which had a $\%Na_2O$ content of 3.1, developed the highest 28-day compressive of 61 MPa. Increasing the content of SS resulted in immediate reductions in compressive strength. Starting at an Ms value of 1.48 and a corresponding $\%Na_2O$ content of 3.1%, the 28-day compressive strength depreciated by 23% when an Ms value of 1.94 and corresponding $\%Na_2O$ content of 4.1% was reached. From both series of samples, a clear correlation can be observed; the highest compressive strengths were attained at a Ms

value between 1.27 and 1.48, while significant reductions in compressive strength were found at Ms values above 1.48, corresponding to a $\%Na_2O$ content of 3.1% and above. Although the best performing samples regarding compressive strength i.e. sample 2 and 7 had the same $\%Na_2O$ contents i.e. 3.1%, the (*a*/*p*) ratio for sample 7 was only 0.22, meaning it contained 27% less activator than sample 2. The latter is apparent since, at the higher *a*/*p* ratio range i.e. 0.34, the compressive strength achieved was significantly reduced regardless of whether the SS/SH ratio was high as in the case of sample 11 (SS/SH = 5.0) or low as in the case of sample 6 (SS/SH = 1.85). Furthermore, when compared to the 100TMW control sample investigated in Stage I, sample 7 was calculated to contain 22.5% less SS. This is based on the reduction in the *a*/*p* ratio from 0.28 to 0.22 and the SS/SH ratio from 4.0 to 2.88. The latter observations lead to the following relationships: (1) samples made with low *a*/*p* ratios i.e. below 0.28 can achieve superior compressive strength when made with an alkali activator consisting of a SS/SH ratio between 2.5 and 5.0, (2) WG can effectively reduce the SS component in AAB systems.

In both series, however, samples prepared with the lowest *a*/*p* ratios did suffer from a 'balling' effect [44] due to the low water/solid ratio. Nonetheless, SEM analyses revealed a highly compact paste microstructure (Fig. 6a) which may partly explain the high compressive strength attained by these samples. The increase in water/solid content has previously been shown to contribute to the reduction of fly ash-based AAB compressive strength due to crystallisation of the otherwise amorphous reaction products [45]. However, in the samples prepared in this study, no products of crystalline nature were observed for the highest water/precursor ratio of 0.23. Instead, at high *a*/*p* ratios, the activating solution was observed to bleed, covering the sample surface and mould. The activator bleeding measured for sample 11 and was determined as 21% of the total activator in the AAB. The latter value of bleeding is significantly large and means only 79% of activator participated in the reaction. Unlike in concrete where the excess bleed water can evaporate without affecting the mechanical strength, the loss of activating solution in AABs is detrimental to the hardening and thus contributes to the lower mechanical strength observed in this study. SEM analyses of samples with a high *a*/*p* ratio support the latter claim by revealing the channel-like paths that formed around particles (Fig. 6b) through which the activator solution was allowed to escape.

The reduced water content of the low *a*/*p* ratio samples was counteracted by the addition of extra mixing water by weight of precursor. In this case, 6, 7 and 8 wt% of water was chosen to be added to sample 7, initially consisting of a water/precursor ratio of 0.14 and SS/SH and *a*/*p* ratio of 2.88 and 0.22, respectively. It can be seen from Fig. 7 that the initial introduction of mixing water led to a slight reduction in the 28-day compressive strength. However the further increase in the mixing water content contributed to restoring the compressive strength, and ultimately at 8 wt% extra mixing water, the compressive strength reached the same value as the control sample (sample 7). The total liquid present in the system originates from the water contained in the activator solution and from the extra mixing water. Thus the total water/precursor ratio of the optimised sample containing extra 8 wt% mixing water was calculated as 0.21. The flow of the pastes with 6, 7, and 8 wt% extra mixing water was 101 ± 5 mm, 116 ± 5 mm and 136 ± 5 mm, respectively. The coarser nature and reduced water

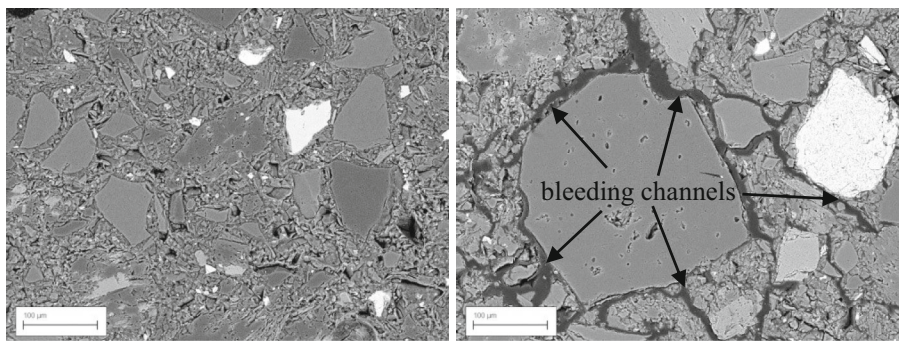

Fig. 6 Images of **a** microstructure of a low *a*/*p* ratio mix, **b** bleeding channels in a high *a*/*p* ratio mix

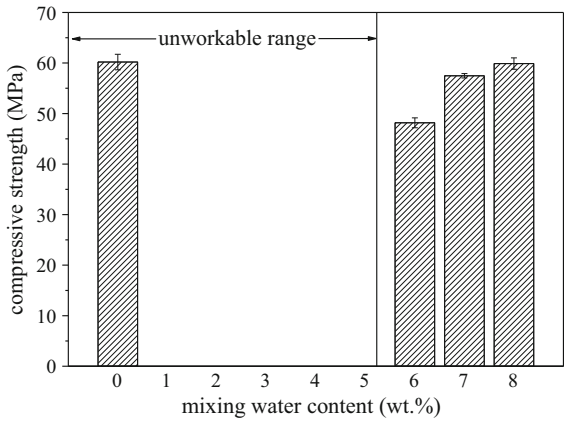

Fig. 7 TMW–WG AAB 28-day compressive strength with varying quantities of mixing water

absorption properties of the WG particles led to the AAB requiring such a low water demand. No bleeding was detected for any of the TMW–WG AAB mixtures. Improvements in compressive strength with an increase in mixing water content at a constant *a*/*p* and SS/SH ratio confirm that the observed reductions in compressive strength shown in Fig. 5 are in fact due to the increased content of $\%Na_2O$ from the activator solution, and not the increase in the water content.

Figure 8 presents the initial and final setting times of all of the samples evaluated in stage II. Samples 1–6 were made with activating solutions of varying SH quantity and a constant SS/precursor ratio while samples 7–11 were made with activating solutions of varying SS quantity and a constant SH/precursor ratio; a horizontal dashed line is included in Fig. 8 to distinguish the two sets. A distinct reduction in initial and final setting time

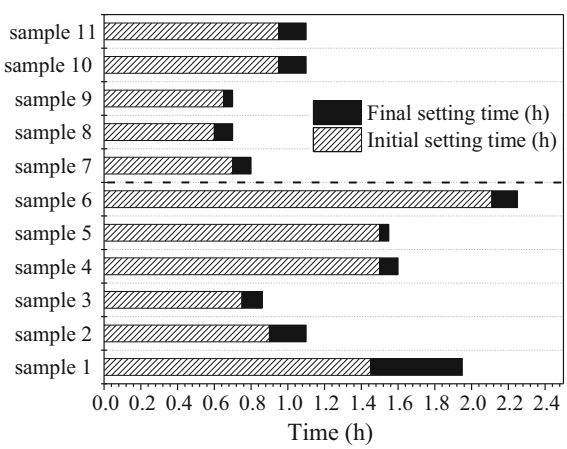

Fig. 8 Initial and final setting times of samples 1–11

can be observed when the activators SH content increases from 0.02 to 0.06 in the samples 1–3, respectively. Further increasing the SH after that leads to an immediate increase in initial setting time while leaving the final setting time largely unaffected, as shown by samples 4 and 5. Sample 6 which contained the highest SH content evaluated in this set of samples and consequently the highest *a*/*p* ratio of 0.34 leads to the slowest initial setting of 2.12 h.

The initial and final setting times of samples 7–11 were far lower than those of samples 1–6. The SS/SH ratio for the samples 7–11 was increasing with an increase in the *a*/*p* ratio however for the samples 1–6, it was the inverse i.e. the SS/SH ratio was increasing with a decrease of the *a*/*p* ratio. The common trend which can be observed in both sets of samples is the fact that the initial setting time increased when the *a*/*p* ratio was greater than 0.28, indicating that the total activator content was the most dominant factor in controlling the AAB setting time. The setting time also appeared to be affected by the SS/SH ratio, however to a lesser extent, and predominately in the samples for which the amount of SH was varied i.e. sample 1–6. As an example, sample 4 which was produced with a SS/SH ratio of 2.7 at an *a*/*p* ratio of 0.3 attained a 28-day compressive strength of 32.5 MPa whereas sample 7 which was produced with an almost identical SS/SH ratio of 2.88 but instead with a lower *a*/*p* ratio of 0.22, attained 61 MPa at 28 days. Sample 7, yielded the initial and final setting times of 42 and 52 min, respectively. With the addition of 8 wt% mixing water, the initial and final setting times slightly increased to 54 and 66 min, complying with EN 196-3:2016 which specifies that the initial setting time should not be less than 45 min while the final setting time should not be more than 10 h. The short time interval between the initial and final setting, but with appropriate initial setting time would make it an ideal candidate for pre-cast fabrication and rapid road repair. It must be noted, however, that these results are valid within the specified range of the process parameters along with their chosen levels and for the specific tungsten mining waste.

4 Conclusions

The influence of the waste glass and alkali activator composition were examined regarding mechanical strength and workability for TMW–WG AAB.

Balance was required between sufficient stimulation of precursor dissolution and avoidance of using highly alkaline conditions due to the associated health risks. Based on these conditions and the results obtained, the following conclusions can be drawn:

- The condition for achieving the highest strength was achieved with a WG replacement by 40 wt%. In combination with the calcium component, the reactive silica led to the formation of (C, N)–A–S–H gel products whilst also providing a 22.5% reduction in the SS content. Thus WG can be considered to impart high strengths with a potential for lower alkali solution demands.
- The TMW/WG blend was successfully cured primarily at room temperature and evaluated to have a low activating solution demand and produced 28-day compressive strength above 42 MPa when an activator/precursor ratio was maintained <0.28.
- The values of Ms for an activator/precursor ratio <0.28 were calculated to be in the 1.48–2.0 range. The lower end of the range i.e. 1.48 proved to be the most economical since it represents the lowest quantity of alkali activator, and also achieved the highest compressive strength i.e. 61 MPa.
- The properties of TMW–WG AAB systems can be drastically affected by minor changes in the alkali activator Na_2O concentrations, values of which should not surpass 3.6% when controlling the SS/SH ratio.
- A water/precursor ratio of 0.21 for TMW–WG AABs resulted in the optimal compressive strength and most satisfactory workability and setting time.

Funding This study was funded by the European Commission Horizon 2020 MARIE Skłodowska-CURIE Research and Innovation Staff Exchange Scheme (Grant Agreement Number 645696). Brunel University London and Thomas Gerald Gray Charitable Trust provided a bursary and fees, respectively to support the first author's Ph.D. study.

Compliance with ethical standards

Conflict of interest The authors declare that they have no conflict of interest.

References

1. ASCEM B.V. (2015) Cement compound and a method for the production thereof. Patent WO/2015/187022
2. Banah UK Ltd (2012) Geopolymeric structural building units and methods of manufacture thereof. Patent 2011003918A1
3. Pappalardo A, Jalali S, Silva FJ (2014) Characterization of parameters to predict the structural behaviour of geopolymeric mortar plates strengthened with carbon fiber reinforced polymer. Key Eng Mater 634:485–497. doi:10.4028/www.scientific.net/KEM.634.485
4. Glasby T, Day J, Genrich R, et al (2015) EFC geopolymer concrete aircraft pavements at Brisbane West Wellcamp Airport. In: Concrete 2015, Melbourne, pp 1–9
5. Duxson P, Fernández-Jiménez A, Provis JL et al (2007) Geopolymer technology: the current state of the art. J Mater Sci 42:2917–2933. doi:10.1007/s10853-006-0637-z
6. Hardjito D, Cheak CC, Ho C et al (2009) Strength and setting times of low calcium fly ash-based geopolymer mortar. Mod Appl Sci 2:P3. doi:10.5539/mas.v2n4P3
7. Thomas RJ, Peethamparan S (2015) Alkali-activated concrete: Engineering properties and stress–strain behavior. Constr Build Mater 93:49–56. doi:10.1016/j.conbuildmat.2015.04.039
8. Ariffin MAM, Bhutta MAR, Hussin MW et al (2013) Sulfuric acid resistance of blended ash geopolymer concrete. Constr Build Mater 43:80–86. doi:10.1016/j.conbuildmat.2013.01.018
9. Lee NK, Lee HK (2015) Reactivity and reaction products of alkali-activated, fly ash/slag paste. Constr Build Mater 81:303–312. doi:10.1016/j.conbuildmat.2015.02.022
10. Khater HM, Abd el Gawaad HA (2016) Characterization of alkali activated geopolymer mortar doped with MWCNT. Constr Build Mater 102:329–337. doi:10.1016/j.conbuildmat.2015.10.121
11. Phetchuay C, Horpibulsuk S, Arulrajah A et al (2016) Spent coffee grounds–fly ash geopolymer used as an embankment structural fill material. J Mater Civ Eng. doi:10.1061/(ASCE)MT.1943-5533.0001496
12. European Commission (2009) Reference document on best available techniques for management of tailings and waste-rock in mining activities. http://eippcb.jrc.ec.europa.eu/reference/mmr.html. Accessed 11 Jan 2017
13. Pacheco-Torgal F, Castro-Gomes J, Jalali S (2008) Properties of tungsten mine waste geopolymeric binder. Constr Build Mater 22:1201–1211. doi:10.1016/j.conbuildmat.2007.01.022
14. Pacheco-Torgal F, Castro-Gomes J, Jalali S (2009) Tungsten mine waste geopolymeric binder: preliminary hydration products investigations. Constr Build Mater 23:31–48. doi:10.1016/j.conbuildmat.2008.01.003
15. Glass for Europe (2013) Recycling of end-of-life building glass. goo.gl/CzmEvs. Accessed 8 Jan 2017
16. Shao Y, Lefort T, Moras S, Rodriguez D (2000) Studies on concrete containing ground waste glass. Cem Concr Res 30:91–100. doi:10.1016/S0008-8846(99)00213-6

17. Christiansen MU, Sutter LL (2013) ACI SP 294—advances in green binder systems. In: Neithalath N, Hicks J (eds) Waste glass for use in geopolymers. ACI, Farmington Hills, MI, pp 31–48
18. Rodríguez ED, Bernal SA, Provis JL et al (2013) Composites effect of nanosilica-based activators on the performance of an alkali-activated fly ash binder. Cem Concr Compos 35:1–11. doi:10.1016/j.cemconcomp.2012.08.025
19. Donatello S, Fernández-Jimenez A, Palomo A (2013) Very high volume fly ash cements: early age hydration study using Na_2SO_4 as an activator. J Am Ceram Soc 96:900–906. doi:10.1111/jace.12178
20. Garcia-Lodeiro I, Fernandez-Jimenez A, Palomo A (2013) Variation in hybrid cements over time. Alkaline activation of fly ash-portland cement blends. Cem Concr Res 52:112–122. doi:10.1016/j.cemconres.2013.03.022
21. Garcia-Lodeiro I, Fernandez-Jimenez A, Palomo A (2013) Hydration kinetics in hybrid binders: early reaction stages. Cem Concr Compos 39:82–92. doi:10.1016/j.cemconcomp.2013.03.025
22. Shi C, Day RL (1995) Acceleration of the reactivity of fly ash by chemical activation. Cem Concr Res 25:15–21. doi:10.1016/0008-8846(94)00107-A
23. Alahrache S, Winnefeld F, Champenois JB et al (2016) Chemical activation of hybrid binders based on siliceous fly ash and Portland cement. Cem Concr Compos 66:10–23. doi:10.1016/j.cemconcomp.2015.11.003
24. Liu LP, Cui XM, He Y et al (2012) The phase evolution of phosphoric acid-based geopolymers at elevated temperatures. Mater Lett 66:10–12. doi:10.1016/j.matlet.2011.08.043
25. Fernández-Jiménez AM, Palomo A, López-Hombrados C (2006) Engineering properties of alkali-activated fly ash concrete. ACI Mater J 103:106–112
26. Fernández-Jiménez A, Palomo A (2003) Characterisation of fly ashes: potential reactivity as alkaline cements. Fuel 82:2259–2265. doi:10.1016/S0016-2361(03)00194-7
27. Fernández-Jiménez A, Palomo A (2005) Composition and microstructure of alkali activated fly ash binder: effect of the activator. Cem Concr Res 35:1984–1992. doi:10.1016/j.cemconres.2005.03.003
28. Cheng H, Lin K-L, Cui R et al (2015) The effects of SiO_2/Na_2O molar ratio on the characteristics of alkali-activated waste catalyst–metakaolin based geopolymers. Constr Build Mater 95:710–720. doi:10.1016/j.conbuildmat.2015.07.028
29. Joshi SV, Kadu MS (2012) Role of alkaline activator in development of eco-friendly fly Ash based geopolymer concrete. Int J Environ Sci Dev 3:417–421. doi:10.7763/IJESD.2012.V3.258
30. Pouhet R, Cyr M (2015) Alkali–silica reaction in metakaolin-based geopolymer mortar. Mater Struct 48:571–583. doi:10.1617/s11527-014-0445-x
31. Kastiukas G, Zhou X, Castro-Gomes J (2016) Development and optimisation of phase change material-impregnated lightweight aggregates for geopolymer composites made from aluminosilicate rich mud and milled glass powder. Constr Build Mater 110:201–210. doi:10.1016/j.conbuildmat.2016.02.029
32. Escalante García JI, Campos-Venegas K, Gorokhovsky A, Fernández A (2006) Cementitious composites of pulverised fuel ash and blast furnace slag activated by sodium silicate: effect of Na_2O concentration and modulus. Adv Appl Ceram 105:201–208. doi:10.1179/174367606X120151
33. Burciaga-Díaz O, Escalante-García JI, Arellano-Aguilar R, Gorokhovsky A (2010) Statistical analysis of strength development as a function of various parameters on activated metakaolin/slag cements. J Am Ceram Soc 93:541–547. doi:10.1111/j.1551-2916.2009.03414.x
34. Criado M, Fernández-Jiménez A, Palomo A et al (2008) Effect of the SiO_2/Na_2O ratio on the alkali activation of fly ash. Part II: 29Si MAS-NMR Survey. Microporous Mesoporous Mater 109:525–534. doi:10.1016/j.micromeso.2007.05.062
35. Kastiukas G, Zhou X, Castro-Gomes JP (2017) Towards preparation conditions for the synthesis of alkali-activated binders using tungsten mining waste. J Mater Civ Eng. doi:10.1061/(ASCE)MT.1943-5533.0002029
36. European Standard (2005) Methods of testing cement—Part 3: determination of setting times and soundness. EN 196-3:2005+A1
37. European Standard (2006) Methods of test for mortar for masonry—Part 3: determination of consistence of fresh mortar (by flow table). EN 1015-3:1999
38. Chen X, Meawad A, Struble LJ (2014) Method to stop geopolymer reaction. J Am Ceram Soc 97:3270–3275. doi:10.1111/jace.13071
39. European Standard (2005) Admixtures for concrete, mortar and grout-Part 4: determination of bleeding of concrete. BS EN 480-4:2005
40. Ismail I, Bernal SA, Provis JL et al (2014) Modification of phase evolution in alkali-activated blast furnace slag by the incorporation of fly ash. Cem Concr Compos 45:125–135. doi:10.1016/j.cemconcomp.2013.09.006
41. Temuujin J, van Riessen A, Williams R (2009) Influence of calcium compounds on the mechanical properties of fly ash geopolymer pastes. J Hazard Mater 167:82–88. doi:10.1016/j.jhazmat.2008.12.121
42. Pacheco-Torgal F, Castro-Gomes JP, Jalali S (2009) Utilization of mining wastes to produce geopolymer binders. In: Provis J, Van Jaarsveld JGS, Van Deventer JSJ (eds) Geopolymers: structure, processing, properties and industrial applications. Woodhead Publishing Limited, Cambridge, pp 267–293
43. Juška G, Arlauskas K, Viliunas M et al (2000) Charge transport in pi-conjugated polymers from extraction current transients. Phys Rev B 62:R16235–R16238. doi:10.1103/PhysRevB.62.R16235
44. Kay EA (2003) Hot and cold weather concreting. In: Newman J, Choo BS (eds) Advanced concrete technology. Butterworth-Heinemann, Oxford, pp 1–18
45. Bakharev T (2005) Geopolymeric materials prepared using Class F fly ash and elevated temperature curing. Cem Concr Res 35:1224–1232. doi:10.1016/j.cemconres.2004.06.031